Response of Block-Copolymer Thin-Film Morphology to Line-Width Roughness on a Chemoepitaxial Template

Paul N. Patrone[*,†] and Gregg. M. Gallatin[*,‡]

Institute for Mathematics and its Applications, University of Minnesota, Minneapolis, Minnesota, 55455, and Center for Nanoscale Science and Technology, National Institute of Standards and Technology, Gaithersburg, Maryland 20899, USA.

E-mail: ppatrone@umn.edu; ggallatin@charter.net

Abstract

Using the Leibler-Ohta-Kawasaki (LOK) phase-field model of block copolymers (BCPs), we characterize how line-width roughness (LWR) in chemoepitaxial template affects the BCP microdomain shape. Specifically, we derive formulas for the monomer density and the microdomain interface profile of periodic, lamellar BCP melts whose template lines widths oscillate with frequency k. The key idea behind our approach is to identify variations in the microdomain interface positions (relative to their averages) as corresponding to a local excess of one of the monomer types. For lamellar systems, our analysis (i) shows that the BCP morphology arises from the constraint that the total mass in a microdomain is fixed, independent of LWR, and (ii) determines a length scale λ over which template LWR affects the substrate.

[*]To whom correspondence should be addressed

[†]Institute for Mathematics and its Applications, University of Minnesota, Minneapolis, Minnesota, 55455, and Center for Nanoscale Science and Technology, National Institute of Standards and Technology, Gaithersburg, Maryland 20899, USA.

[‡]Applied Math Solutions LLC, Newtown, Connecticut 06470

Introduction

Interest in self-assembling block copolymers (BCPs) has increased dramatically in recent years, due in large part to their potential applications in the semiconductor industry. One of the key properties that makes BCPs promising is their ability to self-assemble into microdomains whose size, shape, and spacing are the same as or smaller than features found in modern microprocessors.[1,2] Experiments have also shown that sparse arrays of chemoepitaxial and graphoepitaxial templates can induce long-range order in BCP thin films,[3–6] giving rise to the hope that such systems can be used in the high-fidelity pattern-transfer processes required to make state-of-the-art logic chips.[7–10]

In many applications, chemoepitaxial templates are patterned into the substrate in the form of chemical guiding stripes.[5,6] One of the monomer species preferentially wets this patterned area, causing the microdomains to align parallel to the orientation of the stripes (cf. 1). In real systems, fabrication of chemoepitaxial templates is an imperfect process, and defects such as line-edge roughness (LER) and line-width roughness (LWR) often appear in the guiding stripes themselves. In assessing the usefulness of BCPs for industrial applications (where defects in the final product are unacceptable), it is therefore critical to understand how imperfections in the template propagate into the polymer melt.

In this paper, our goal is to analytically describe the response of lamellar BCP thin films to LWR in chemoepitaxial templates. Specifically, we derive simple formulas for the three-dimensional morphology of lamellar microdomains on top of periodically spaced, parallel template lines whose mean width and separation are equal to the preferred BCP microdomain width (see 1). Our analysis, which is based on the Leibler-Ohta-Kawasaki phase field model,[11–13] yields a length-scale $\lambda^{-1} \sim R_g$ (where R_g is the radius of gyration) over which long-wavelength defects on the substrate propagate into the melt and suggests that the microdomain morphology is determined largely by a fixed-mass constraint, i.e. a requirement that the total mass in a microdomain is constant, independent of LWR.[14]

The main physical idea behind our approach is to identify variations in the microdomain

interface positions (relative to their averages) as corresponding to a local excess of one of the monomer types. Analytically, this is achieved by a variational-type approach. Specifically, we assume that the relative monomer density ϕ can be written in a form corresponding to lamellar microdomains, but with the interface positions given by an unknown function f. Expressing the LOK free energy in terms of f then yields an equation that is exactly solvable. Importantly, our analysis shows how the fixed-mass constraint is an intrinsic element the equation for f, and consequently the LOK model.

We emphasize that the cause of LWR considered here is distinct from thermal fluctuations, which can also lead to roughening of the microdomain interfaces.[15,16] In this work, we introduce LWR implicitly through the use of appropriate boundary conditions that model the BCP-substrate interaction. While this approach may seem *ad hoc*, the features of real chemoepitaxial templates have their own LER and LWR (see, for example, Fig. 4 of [22]), which alters the BCP microdomain morphology. Understanding the effects of such template roughness is critically important for industrial applications, where the *total* roughness (arising from all sources) must be bounded.[10,17] Moreover, Perera *et al.* have suggested that non-uniform domain shapes can lead to unreliable pattern transfer during plasma etching of the BCP patterns,[22] which underscores the need to better understand the role of substrates in determining the BCP morphology.

Other works have considered related questions concerning the role of template defects on BCP morphology.[18–24] In particular, Refs. [18] and [19] used Monte Carlo simulations to characterize the effects of template confinement and pitch multiplication on BCP morphology, while Ref [20] used self-consistent field simulations to study similar problems for polymer brushes on the substrate. Moreover, Refs. [21–24] used molecular-level simulations and field-theoretic techniques to describe how defects in the template propagate into the melt. Notably, Ref. [24] also formulated an analytical model, based on the energetics of curved surfaces, to describe the microdomain interface shape; cf. related models in Ref. [25]. Our approach differs from past works insofar as we analytically derive and solve a model of the

microdomain geometry using the LOK phase-field model.[12,26] Given that the LOK model does not explicitly describe the microdomain interfaces, it is interesting to note that our main results are consistent with phenomena described by the analytical model in Ref. [24]. Our main results are also in agreement with the small-angle x-ray scattering experiments in Ref. [18].

We emphasize that while our main findings can be expressed with simple formulas, our analysis necessarily invokes simplifying assumptions that may limit our results. In particular, we assume that the BCP microdomains conform exactly to the template geometry, neglecting the possibility that the polymers may not entirely wet the template or follow higly distorted patterns. Moreover, the LOK model itself, as well as our application of it to confined systems, is a simplification of the the full self-consistent field theory described in, e.g. Ref. [13], and our analysis relies on approximate minimizers of the LOK functional (although this approach was first advocated by Ohta and Kawasaki).[12,27] Nonetheless, the success of the LOK model in describing equilibrium properties of BCPs, as well as the agreement we find with experimental results, leads us to believe that our results are useful for understanding systems where the template LWR is small, but not negligible.[15]

Elements of the Model

We consider a system of straight and parallel (on average) lamellae in the strong segregation regime (SSR); see 1. Let x and y both be parallel to the substrate, with x perpendicular to the mean interface positions and y parallel to the mean interface positions; let z be perpendicular to the substrate. We denote the average width and height of the lamellae by ℓ and h, and assume that the system is periodic (with a period of 2ℓ) in x, infinite in y, and finite in z. We take the $z = 0$ and $z = h$ planes to be the substrate and a neutral top-coat. On the substrate, we assume that there are periodically spaced, chemoepitaxial stripes whose centers are parallel to the y axis. The spacing between the centers of the stripes is 2ℓ, and

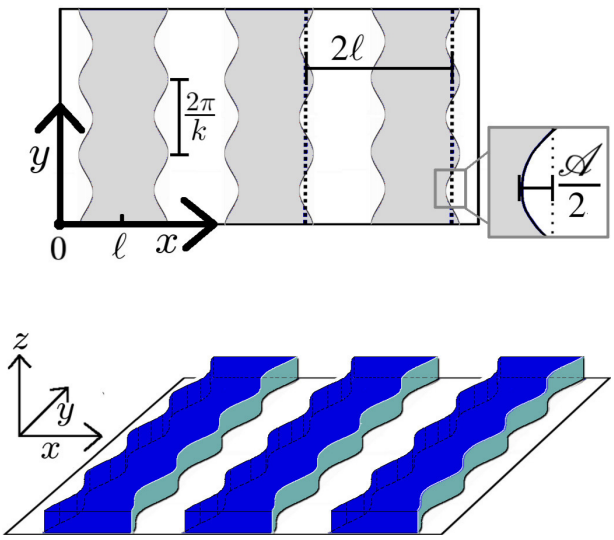

Figure 1: (a) Top-down view of a substrate with a chemoepitaxial pattern (gray). We consider the effects of a pattern with line-width roughness having a wavelength $2\pi/k$. (b) After adding polymers to the system, the A polymers (blue) self-assemble over the chemical patterns, while the B polymers (not shown) assemble over the non-patterned substrate. Our key goal is to determine the 3D morphology of the microdomains as a function of the wavelength $2\pi/k$.

we assume that the stripe widths oscillate with an amplitude $\mathcal{A}$ and frequency k about the mean value ℓ .

The LOK model describes this system in terms of the relative density of monomers $\phi(x, y, z)$, where $-1 \leq \phi \leq 1$; $\phi = \pm 1$ correspond to pure A (+) and B (-) domains. The state of the system is governed by a free energy $\mathcal{F}[\phi]$ whose minimizer $\hat{\phi}$ describes one of the possible BCP phases, depending on the relative fraction $\hat{f}$ of A and B monomers. The functional $\mathcal{F}[\phi]$ is given by

$$\mathcal{F}[\phi] = \chi k_B T \int_V \mathrm{dV}\, \frac{\xi^2}{2}(\nabla\phi)^2 - \frac{\phi^2}{2} + \frac{\phi^4}{4} + \frac{\varsigma}{2}\int_V \mathrm{dV} \int_{V'} \mathrm{dV}'\phi(\mathbf{r}')G(\mathbf{r}', \mathbf{r})\phi(\mathbf{r}) \tag{1}$$

where χ is the Flory-Huggins parameter (which characterizes the A-B repulsion strength). The parameter $\xi := \{a^2/[3\hat{f}(1-\hat{f})\chi]\}^{1/2}$ is proportional to the A-B interface width, and $\varsigma := 36/\hat{f}^2(1-\hat{f})^2 a^2 \chi \mathcal{N}^2$ describes the strength of nonlocal, steric interactions between

polymer chains. In the above expressions, $\mathcal{N}$ is the index of polymerization, and a is the Kuhn statistical length; here we set $\hat{f} = 1/2$ (i.e. equal volume fraction of A and B monomers). The $G(\mathbf{r}', \mathbf{r})$ is the Green's function of the Laplacian chosen to satisfy Neumann boundary conditions on the x and z boundaries, i.e.,

$$G(\mathbf{r}', \mathbf{r}) = \sum_{k_x,k_z} \int \frac{dk_y}{2\pi} \frac{\cos(k_x x)\cos(k_x x')\cos(k_z z)\cos(k_z z')e^{ik_y(y-y')}}{\ell h(k_x^2 + k_y^2 + k_z^2)(1+\delta_{k_x,0})(1+\delta_{k_z,0})}, \tag{2}$$

where $\delta_{j,k}$ is the Kronecker delta, $k_x = m\pi/2\ell$, and $k_z = n\pi/h$, with $m, n = 1, 2, ...$ We note that the use of the non-local term in Eq. (1) amounts to an assumption on the form of the energy functional for thin films; see the Discussion section for more details.

In order to find an equation for the minimum energy configuration, we write $\phi = \hat{\phi} + \delta\phi$, where $\hat{\phi}$ is assumed to minimize Eq. (1) and $\delta\phi$ is a variation of $\hat{\phi}$ that vanishes on $z = 0$ and when $y \to \infty$. Since the top-coat is neutral, we do not fix the microdomain interface positions on $z = h$; this corresponds to letting $\delta\phi$ to vary on $z = h$. Substituting $\hat{\phi} + \delta\phi$ for ϕ in Eq. (1) and applying integration by parts, we set the first variation (i.e. terms multiplying $\delta\phi$) equal to zero to find that $\hat{\phi}$ satisfies

$$0 = -\xi^2\nabla^2\hat{\phi} - \hat{\phi} + \hat{\phi}^3 + \varsigma \int_{V'} \mathrm{dV}' G(\mathbf{r}, \mathbf{r}')\hat{\phi}(\mathbf{r}') \tag{3}$$

subject to the boundary conditions

$$\hat{\phi}(0, y, z) = \hat{\phi}(2\ell, y, z), \tag{3a}$$

$$\partial_z\hat{\phi} = 0, \qquad z = h, \tag{3b}$$

$$\hat{\phi}(x, y, 0) = 1, \qquad (x, y) \in S, \tag{3c}$$

$$\hat{\phi}(x, y, 0) = -1, \qquad (x, y) \in B, \tag{3d}$$

where S is the chemoepitaxial stripe [(x, y) for which $\ell/2 - (\mathcal{A}/2)\cos(ky) \leq x \leq 3\ell/2 +$

$(\mathcal{A}/2)\cos(ky)]$, and B is the bare substrate $[(x,y)$ for which which $x < \ell/2 - (\mathcal{A}/2)\cos(ky)$ or $x > 3\ell/2 + (\mathcal{A}/2)\cos(ky)]$. Boundary condition (3b) is a consequence of the assumption that the top-coat is neutral;[29] physically, this boundary condition states that neither monomer species tends to increase near (i.e. be attracted to or repulsed by) the top-coat.

Analysis of the Model

In the spirit of Ref. [12], we propose the trial function

$$\hat{\phi} = 1 - \tanh\left[\frac{2x - \ell + f(y,z)}{2\sqrt{2}\xi}\right] + \tanh\left[\frac{2x - 3\ell - f(y,z)}{2\sqrt{2}\xi}\right], \tag{4}$$

on the domain $0 \leq x \leq 2\ell$, where $f(y,z)$ is an unknown function. Physically, Eq. (4) corresponds to a lamellar density profile, but with the microdomain interfaces shifted from their bulk positions by $f/2$; cf. 2. We assume that $|f(y,z)| \ll \ell$ so that two adjacent interfaces never touch.[28] Consequently, $\hat{\phi}$ solves the nonlinear equation $-\xi^2\partial_x^2\phi - \phi + \phi^3 = 0$ up to exponentially small corrections (cf. the Appendix), which reduces Eq. (3) to

$$0 = -\xi^2(\nabla_\rho^2)\hat{\phi} + \varsigma \int_{V'} \mathrm{d}V' G(\mathbf{r},\mathbf{r}')\hat{\phi}(\mathbf{r}'), \tag{5}$$

where $\boldsymbol{\rho} = (y,z)$ and $\nabla_\rho = (\partial_y, \partial_z)$.

In order to simplify Eq. (5), note that $\hat{\phi}$ is approximately a pair of step functions (ranging from -1 to 1) in the SSR, when $\xi \ll \ell - |f(y,z)|$ (cf. 2); thus, to exponentially small corrections we find that

$$f(y,z) \approx \frac{1}{2}\int_0^{2\ell} \mathrm{d}x\, \hat{\phi}(x,y,z). \tag{6}$$

Equation (6) is a key identity; physically, it states that the relative excess of monomers on any line with fixed y and z is proportional to the shift in the microdomain interface positions.

Integrating Eq. (5) with respect to x, we invoke Eq. (6) to find an equation for f,

$$0 = -\nabla_\rho^2 f + \lambda^4 \int \mathrm{d}\boldsymbol{\rho}'\, g(\boldsymbol{\rho}', \boldsymbol{\rho}) f(\boldsymbol{\rho}'), \tag{7}$$

with the boundary conditions

$$\partial_z f\big|_{z=h} = 0 \qquad\qquad f(y, 0) = \mathcal{A}\cos(k\, y) \tag{8}$$

where $\lambda = (\varsigma/\xi^2)^{1/4}$ and $g(\boldsymbol{\rho}', \boldsymbol{\rho}) = \int_0^{2\ell} \mathrm{d}x\, G(\mathbf{r}', \mathbf{r})$ is a 2-dimensional Green's function [cf. the Appendix for a brief discussion of $g(\boldsymbol{\rho}', \boldsymbol{\rho})$]. Note that $\lambda \sim 1/R_g$, where R_g is the radius of gyration.

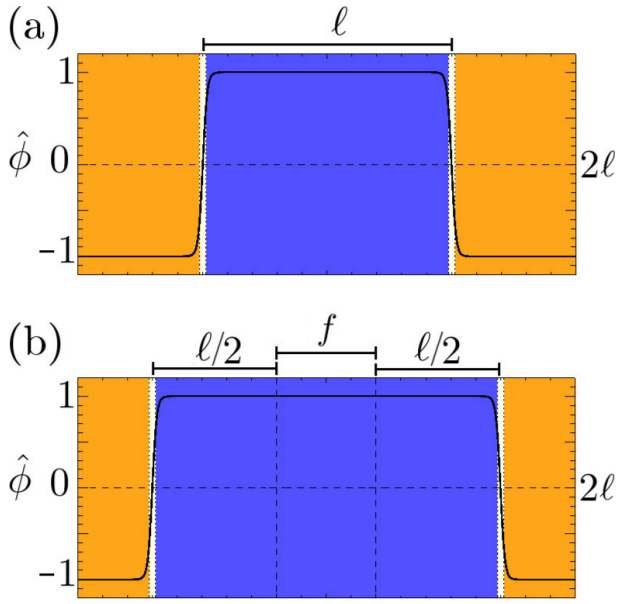

Figure 2: Plot of $\hat{\phi}$ [cf. Eq. (4)] as a function of x when (a) $f(y, z) = 0$ and (b) $f(y, z) = 2\ell/5$. The density $\hat{\phi}$ is approximately a step function that changes values at $\ell/2 - f(y, z)/2$ and $3\ell/2 + f(y, z)/2$. The boundary layer (yellow) separating microdomains has a width of roughly $2\sqrt{2}\xi \ll \ell$ in the SSR. Thus, we approximate $f(y, z) \approx (1/2)\int_0^{2\ell} \mathrm{d}x\, \hat{\phi}(x, y, z)$.

We now proceed to solve for f exactly. Exploiting the property that $\nabla_\rho^2 g(\boldsymbol{\rho}', \boldsymbol{\rho}) = -\delta(\boldsymbol{\rho} - \boldsymbol{\rho}')$, we apply ∇_ρ^2 to (7), which yields the constant-coefficient equation

$$(\partial_{yyyy} + 2\partial_{yyzz} + \partial_{zzzz}) f + \lambda^4 f = 0. \tag{9}$$

Writing $f = \cos(k\,y)e^{\alpha z}$, it is straightforward to show that (9) α satisfies the algebraic equation

$$\alpha^4 - 2k^2\alpha^2 + (k^4 + \lambda^4) = 0, \tag{10}$$

which has the solutions

$$\begin{aligned} \alpha_1 &= \sqrt{k^2 + i\lambda^2} & \alpha_2 &= -\sqrt{k^2 + i\lambda^2} \\ \alpha_3 &= \sqrt{k^2 - i\lambda^2} & \alpha_4 &= -\sqrt{k^2 - i\lambda^2}. \end{aligned} \tag{11}$$

Thus, the general solution to (9) can be written as

$$f = \mathcal{C}_j e^{\alpha_j z} \cos(k\,y), \tag{12}$$

where $\mathcal{C}_j$ are unknown constants (summation implied over repeated indices).

We pause to discuss the interpretation of f. Since $f(y,0) = \mathcal{A}\cos(k\,y)$, the interface position oscillates with the chemoepitaxial template along the substrate. As z increases, the contribution to f coming from the $e^{\alpha_j z}$ determines whether the amplitude of the interface oscillation changes in magnitude and/or sign. In the limit that $k \to \infty$, one finds that $\alpha_j \to \pm k$, so that the interface fluctuation amplitude either decays or grows exponentially. As $k \to 0$, $\alpha_j \to \pm(\lambda \pm i\lambda)/\sqrt{2}$, and the interface amplitude can undergo a sign change.

Since (12) has four unknown coefficients, while the general solution to (7) should only have two, we require two additional constraints on the $\mathcal{C}_j$ in order to uniquely determine f. We find such constraints by inserting (12) into (7) and using integration by parts to eliminate the nonlocal term. Specifically, note that

$$\Phi := \sum_j \frac{\mathcal{C}_j e^{\alpha_j z}\cos(ky)}{\alpha_j^2 - k^2} \tag{13}$$

solves $\nabla_\rho^2 \Phi = f(\boldsymbol{\rho})$. Using this fact, we rewrite (7) as

$$0 = -\nabla_\rho^2 f + \lambda^4 \int \mathrm{d}\boldsymbol{\rho'}\; g(\boldsymbol{\rho'}, \boldsymbol{\rho})\, \nabla_{\rho'}^2 \Phi(\boldsymbol{\rho'}) \tag{14}$$

and apply integration by parts twice to yield

$$\int_{-\infty}^{\infty} \mathrm{d}y' g(y, z, y', z') \partial_{z'} \Phi(y', z') \Big|_{z'=0}^{z'=h} = 0. \tag{15}$$

Since in general this integral is a function of z, we find the two additional constraints that $\partial_z \Phi(y, z) = 0$ for $z = 0$ and $z = h$. The four equations for $\mathcal{C}_j$ are then

$$\sum_j \mathcal{C}_j = \mathcal{A}, \qquad \sum_j \mathcal{C}_j \alpha_j e^{\alpha_j h} = 0, \tag{16}$$

$$\sum_j \frac{\mathcal{C}_j \alpha_j}{\alpha_j^2 - k^2} = 0, \qquad \sum_j \frac{\mathcal{C}_j \alpha_j e^{\alpha_j h}}{\alpha_j^2 - k^2} = 0. \tag{17}$$

Equations (16) restate Eqs. (8), while Eqs. (17) are equivalent to $\partial_z \Phi(y, z) = 0$ for $z = 0$ and $z = h$.

Solving the system of equations (16)–(17) yields the coefficients $\mathcal{C}_j$. We leave the details of this algebra to the interested reader and note only the results

$$\mathcal{C}_1 = -(\mathcal{A}/\mathcal{D}) \alpha_2 \alpha_3 \alpha_4 \left[e^{(\alpha_2 + \alpha_3)h} - e^{(\alpha_2 + \alpha_4)h} \right], \tag{18}$$

$$\mathcal{C}_2 = (\mathcal{A}/\mathcal{D}) \alpha_1 \alpha_3 \alpha_4 \left[e^{(\alpha_1 + \alpha_3)h} - e^{(\alpha_1 + \alpha_4)h} \right], \tag{19}$$

$$\mathcal{C}_3 = -(\mathcal{A}/\mathcal{D}) \alpha_1 \alpha_2 \alpha_4 \left[e^{(\alpha_1 + \alpha_4)h} - e^{(\alpha_2 + \alpha_4)h} \right], \tag{20}$$

$$\mathcal{C}_4 = (\mathcal{A}/\mathcal{D}) \alpha_1 \alpha_2 \alpha_3 \left[e^{(\alpha_1 + \alpha_3)h} - e^{(\alpha_2 + \alpha_3)h} \right], \tag{21}$$

where $\mathcal{D}$ is a normalizing constant subject to the constraint that $\sum_{i=1}^4 \mathcal{C}_i = \mathcal{A}$. Inspection of Eqs. (18)–(21) reveals that the coefficients $\mathcal{C}_2$ and $\mathcal{C}_4$ dominate the behavior of f by virtue of the fact that $\alpha_2 = -\sqrt{k^2 + i\lambda^2}$ and $\alpha_4 = -\sqrt{k^2 - i\lambda^2}$ suppress $\mathcal{C}_1$ and $\mathcal{C}_3$. Moreover, closer

examination of Eqs. (17) and the asymptotic forms of α reveal important information about the physics of defect propagation. In particular, when $k \to 0$ (i.e. as the wavelength of the template oscillations goes to infinity), Eqs. (17) become $\sum_j \mathcal{C}_j/\alpha_j = \sum_j \mathcal{C}_j e^{\alpha_j h}/\alpha_j = 0$, which implies $\int_0^h \mathrm{d}z\, f(y,z) = 0$ for any y. *Physically, this amounts to the fixed-mass constraint, i.e. the requirement that the total mass of monomers be independent of the template line widths.* In this limit, $\alpha_2 \to -(\lambda + i\lambda)/\sqrt{2}$ and $\alpha_4 \to -(\lambda - i\lambda)/\sqrt{2}$; this implies that amplitude of LWR (i.e. f) both decays over the distance R_g and changes sign, since mass must be pulled from above the substrate to compensate for any widening of the microdomains at $z = 0$ (cf. 3).

When $k \neq 0$, oscillations in the template ensure all microdomains have constant mass when integrated over y. When k is small (i.e. long wavelength oscillations of the template), the polymers cannot easily redistribute mass by stretching horizontally, since they are finite length and attached the the substrate; hence, LWR tends to propagate vertically (i.e. the α are dominated by $\lambda \sim R_g^{-1}$). When k is large (i.e. short wavelength oscillations of the template), defects are more effectively damped in the vertical direction since horizontal stretching of the BCPs can accommodate the substrate LWR; analytically, this is seen in that k dominates λ in the α.

Given that the LOK energy functional does not explicitly describe microdomain interfaces, it is interesting to note that, under certain conditions, the analytical model of Ref. [24] agrees with several of our predictions. Specifically, when the interface and substrate are assumed not to be perpendicular, their model predicts the sign change illustrated in our Fig. 3. Moreover, in the limit that $k \to \infty$, Eq. (24) of Ref. [24] predicts that the decay length of deformations is proportional to k^{-1}, whereas in the reverse limit (i.e. $k \to 0$), the decay length is proportional to $\ell \sim R_g^p$, where $p = 1$ in the weak segregation regime and $p = 4/3$ in the SSR.

Discussion

Implications for thin film systems

Block-copolymer systems of interest to industry are typically thin film systems, which are especially susceptable to defects in the underlying template. In such systems, one typically distinguishes between two types of fluctuations, long and short wavelength, where the notion of size is relative to the microdomain periodicity 2ℓ. In this section, we explore the consequences of our main results for thin films with both types of fluctuations.

In Fig. 3, we plot $f(0, z)$ for two different values of k that are representative of short and long wavelength deformations. The inset shows a side view of the BCP melt (cf. Fig. 4 for a three-dimensional representation of the interfaces). Here we have chosen the film height to be equal to the microdomain width ($h = \ell$) and set $\lambda = 8/\ell$. The amplitude of the template LWR has been chosen to be unrealistically large ($\mathcal{A} = \ell/5$) in order to emphasize features of the microdomain boundary. However, the amplitude of the fluctuation f scales linearly with $\mathcal{A}$, so that the following considerations remain independent of our choice.

When, $k \gtrsim \lambda$, the LWR falls to zero at around 30% of the film thickness. Interestingly, when $k < \lambda$, the LWR persists nearly to the top of the film, and the amplitude of LWR changes sign. For a system with $\mathcal{N} \approx 300$, $\xi \approx 1$ nm, and $\chi \approx 0.1$ (corresponding roughly to PS-PDMS [poly(styrene-b-dimethylsiloxane)] with $\ell \approx 10$ nm), we can expect that $\lambda \approx 1$ nm^{-1} (which is close to the value $\lambda = 8/\ell$ in the figure when $\ell = 10$ nm). Hence, for short LWR fluctuations with wavelengths of $2\pi/k \lesssim 8$ nm, we expect the corresponding effect in the BCP microdomains to die off fairly quickly. However, for longer LWR wavelengths $2\pi/k \gtrsim 8nm$, we expect the template to affect the thin film through its entire height. This is the most damaging type of roughness with respect to device performance, since in this case, error in the edge position will be transferred directly into the device structure during subsequent processing.

The presence of a "foot" where the microdomain interface meets the substrate is char-

acteristic of both curves in Fig. 3. This morphological feature has been observed both in numerical simulations of Ref. [21] as well as in the small-angle x-ray scattering (SAXS) experiments of Ref. [18]. The latter work in particular noted that the BCP foot was likely due to penetration of the BCPs into the template brush, which is consistent with our explanation that particles must be drawn from above the substrate in order to wet it fully. Moreover, analysis of the microdomain profiles in Ref. [18] suggested that there is a sign change in the amplitude of the interface fluctuation when moving vertically away from the substrate.

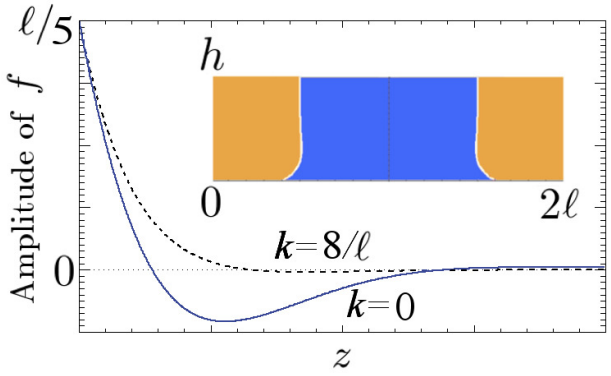

Figure 3: The amplitude $f = \mathcal{C}_j e^{\alpha_j z}$ for $k = 0$ (solid line) and $k = 8/\ell$ (dashed line). These solutions are found by solving the system of equations 16 and (17) for $\mathcal{C}_j$. Here we set $\lambda = 8/\ell$, $\mathcal{A} = \ell/5$, and $h = \ell$. The colored inset shows the $y = 0$ cross section of a BCP microdomain corresponding to the $k = 8/\ell$ mode.

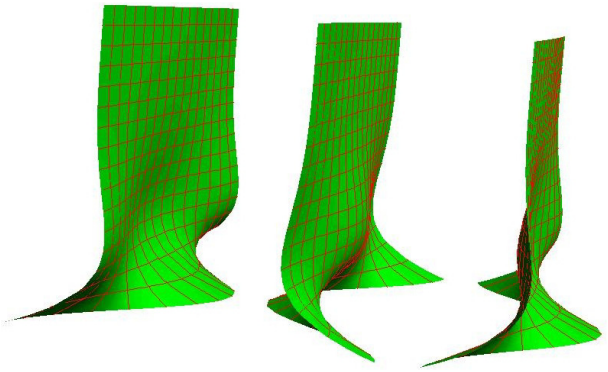

Figure 4: Three-dimensional plots of three microdomain interface boundaries, corresponding to the case $k = 4/\ell$ and $\mathcal{A} = 2\ell/5$ (other parameters the same as in 3).

Generalization of the analysis

Our approach of modeling the microdomain shape in terms of the interface position can easily be generalized to LWR that is not periodic along the length of the guiding stripes. In particular, Eq. (3) always reduces asymptotically to Eq. (5) provided $|f| \ll \ell$, and use of the key identity Eq. (6) is likewise independent of the actual form of f. Consequently, the *linear* Eq. (7) can be used to describe the effects of arbitrary LWR (provided its amplitude is sufficiently small) by expanding the boundary condition Eq. (8) in Fourier modes.

We speculate that it is possible to extend our analysis to the case of pitch multiplication, i.e. to cases where the template stripes have a periodicity of $n\ell$, $n = 4, 6, ...$ (corresponding to a doubling, tripling, etc. of the feature density). Generally speaking, this could be achieved by integrating Eq. (5) over each microdomain separately, yielding a system of coupled PDEs for the individual microdomain positions. However, the resulting equations would likely need to be solved numerically owing to the non-local term in Eq. (5). Moreover, it is not obvious how mass would be distributed amongst non-symmetric microdomains, which would necessitate a careful consideration of boundary conditions over the untemplated substrate.

Limitations of the analysis

Our analysis here does have limitations insofar as we only study periodic arrays of guiding stripes, each having the same LWR. Real chemoepitaxial templates also exhibit LER (shifting of the stripe center without change in width). It is not clear how our analysis could be extended to such situations, since our key identity Eq. (6) only relates $\hat{\phi}$ to f via changes in the microdomain width.

Additionally, we make an assumption that the BCP microdomains are pinned to the chemoepitaxial template, irrespective of how distorted its features may be. While it is likely that the BCP microdomains can conform to slowly varying features, our assumption may not be valid for templates whose features oscillate rapidly. Moreover, we neglect the possibility that the boundary could affect the BCP microdomain interfacial width.

We also emphasize that it is not well understood what specific form, if any, the nonlocal term entering Eq. (1) should take for thin film systems. Here we have used the Green's function that satisfies Neumann boundary conditions, although this choice is not unique. The original derivation of the energy functional applied to bulk systems that were also periodic, and so did not address the question of how polymer chains would interact with and be constrained by surfaces.[12] Reference [30] revisited this problem with the aim of clarifying the key assumptions behind LOK's derivation. They also proposed Neumann conditions as a suitable choice for finite domains, but noted that, "... the interior of the material is not signifcantly affected by the boundary conditions," suggesting that they were not considering thin films. However, it is important to note that the steps leading from Eq. (7) to Eq. (15) do not invoke the boundary conditions on the Green's function (cf. the Appendix). Thus, while we have assumed the specific form of the nonlocal term appearing in the LOK functional, our analysis is more general than suggested by Eq. (1).

Conclusions

In this paper, we derived analytic formulas, based on the LOK model, that describe how the lamellar, BCP microdomain morphology responds to LWR in a periodic, chemoepitaxial template. We determined a lengthscale $\lambda^{-1} \sim R_g$ over which long-wavelength defects propagate into the BCP melt. For shorter wavelength defects, this lengthscale becomes $(k^2 + i\lambda^2)^{-1/2}$, where k is the frequency of the template LWR. Using this result, we showed that the microdomain shape is determined by the ability of the BCPs to accommodate the template LWR by stretching. Open issues include ways to generalize our techniques to non-periodic systems and templates with LER.

Acknowledgements. PNP was supported by the National Institute of Standards and Technology American Recovery and Reinvestment Act Measurement Science and Engineering Fellowship Program Award No. 70NANB10H026 through the University of Maryland. This

author was also supported by the Institute for Mathematics and its Applications at the University of Minnesota. The authors wish to thank Dionisios Margetis, Mark Stiles, and "Charlie" Chi-chun Liu for useful discussion during preparation of this manuscript.

Appendix

In the Appendix, we clarify several mathematical details mentioned in the main text.

On exponential corrections

We begin by showing what it means for Eq. (4) to solve

$$-\xi^2\partial_x^2\phi - \phi + \phi^3 = 0 \tag{22}$$

up to exponentially small corrections. First, note that $\phi = \tanh[(2x - \ell + f)/(2\sqrt{2}\xi)]$ solves Eq. (22) (where f is independe of x), subject to the conditions $\phi \to \pm 1$ as $x \to \pm\infty$. In the limit that $\xi \to 0$, the function ϕ rapidly rises from -1 to 1 in a region having a width $\mathcal{O}(\xi)$ centered at $x = \ell/2 - f/2$. Such transition regions represent the microdomain boundaries.

Now, Eq. (4) is a *linear* combination of three solutions to a *nonlinear* partial differential equation (PDE). Thus, we are not guaranteed (and indeed it is not even expected!) that such a function will solve Eq. (22), owing to the ϕ^3 term. We can compute the the error δ in this approximation by plugging Eq. (4) into Eq. (22) to find the remainder

$$\delta = \hat{\phi}^3 - 1 + \tanh\left[\frac{2x-\ell+f(y,z)}{2\sqrt{2}\xi}\right]^3 - \tanh\left[\frac{2x-3\ell-f(y,z)}{2\sqrt{2}\xi}\right]^3. \tag{23}$$

Next, divide the interval $D = [0, 2\ell]$ into the two partitions $D_l = [0, \ell]$ and $D_h = [\ell, 2\ell]$. Note that for a system in the strong-segretation regime, the separation $\ell - f$ between microdomain boundaries must be large relative to their thickness, which is $\mathcal{O}(\xi)$. This implies that in the

domain D_l, the sum

$$s_l = -1 - \tanh\left[\frac{2x - 3\ell - f(y,z)}{2\sqrt{2}\xi}\right]^3 \lesssim \mathcal{O}\left[\exp(-\ell C/\xi)\right] \tag{24}$$

is exponentially small [where $C = \mathcal{O}(1)$], owing to the fact that the tanh ≈ -1. By expanding $\hat{\phi}^3$ and simplifying Eq. (23), one finds that the error is bounded by terms that are $\mathcal{O}(s_l)$ or smaller. Similar arguments can be used to show that in the domain D_h, the error is bounded by terms that are $\mathcal{O}(s_h)$, where

$$s_h = -1 + \tanh\left[\frac{2x - \ell + f(y,z)}{2\sqrt{2}\xi}\right]^3, \tag{25}$$

is exponentially small as described above.

On the function $g(\boldsymbol{\rho}, \boldsymbol{\rho}')$

The function $g(\boldsymbol{\rho}, \boldsymbol{\rho}')$ is defined via the relation $g(\boldsymbol{\rho}', \boldsymbol{\rho}) = \int_0^{2\ell} \mathrm{d}x\, G(\mathbf{r}', \mathbf{r})$, where $G(\mathbf{r}', \mathbf{r})$ is the full 3-dimensional Green's function given by Eq. (2). Here we briefly show how the relation $\nabla_\rho^2 g(\boldsymbol{\rho}', \boldsymbol{\rho}) = -\delta(\boldsymbol{\rho} - \boldsymbol{\rho}')$ can be derived from Eq. (2).

First, note that $\nabla_{\mathbf{r}}^2 G(\mathbf{r}', \mathbf{r}) = -\delta(\mathbf{r} - \mathbf{r}')$ by definition [or, equivalently, by applying $\nabla_{\mathbf{r}}^2$ to Eq. (2)]. Integrating $\int_0^{2\ell} G(\mathbf{r}, \mathbf{r}')$ and using Eq. (2), one finds that only the terms for which $k_x = 0$ contribute to the sum over k_x and k_y, which yields the expression

$$g(\boldsymbol{\rho}, \boldsymbol{\rho}') = \sum_{k_z} \int \frac{dk_y}{2\pi} \frac{\cos(k_z z)\cos(k_z z') e^{ik_y(y-y')}}{h(k_x^2 + k_y^2 + k_z^2)(1 + \delta_{k_z,0})}. \tag{26}$$

Lastly, applying the operator ∇_ρ^2 to this series yields the corresponding expansion for the delta function in 2-dimensions. Note that this analysis also applies to a Green's function satisfying periodic boundary conditions.

References

(1) Ruiz, R.; Kang, H.; Detcheverry, F. A.; Dobisz, E.; Kercher, D. S.; Albrecht, T. R.; de Pablo, J. J.; Nealey, P. F., *Science* **2008**, *321*, 936–939.

(2) Detcheverry, F. A.; Liu, G.; Nealey, P. F.; de Pablo, J. J., *Macromolecules* **2010**, *43*, 3446–3454.

(3) Sanders, D. P.; Cheng, J.; Rettner, C. T.; Hinsberg, W. D.; Kim, H.; Truong, H.; Friz, A.; Harrer, S.; Holmes, S.; Colburn, M., J. Photopolym. Sci. Technol. **2010,** *23*, 11-18.

(4) Jeong, J. W.; Park, W. I.; Kim, M.; Ross, C. A.; Jung, Y. S., Nano Lett. **2011,** *11*, 4095-4101.

(5) Cheng, J. Y.; Rettner, C. T.; Sanders, D. P.; Kim, H.; Hinsberg, W. D., Adv. Mater. **2008,** *20*, 3155-3158.

(6) Cheng, J. Y.; Ross, C. A.; Smith, H. I.; Thomas, L., Adv. Mater. **2006,** *18*, 2505-2521.

(7) Park, C.; Yoon, J.; Thomas, E. L., Polymer **2003,** *44*, 6725-6760.

(8) Segalman, R. A.; Mater. Sci. Eng. R **2005,** *48*, 191-226.

(9) Darling, S. B., Prog. Polym. Sci. **2007,** *32*, 1152-1204.

(10) *International Technology Roadmap for Semiconductors, 2011 Edition*, http://www.itrs.net/Links/2011ITRS/Home2011.htm.

(11) Leibler, L., Macromolecules **1980,** *13*, 1602-1617.

(12) Ohta, T.; Kawasaki, K., Macromolecules **1986,** *19*, 2621-2632.

(13) Fredrickson, G. H., *The Equilibrium Theory of Inhomogeneous Polymers*; Oxford Science Publications: Oxford, 2006, p. 159.

(14) Loosely speaking, this may be thought of as a "mass conservation" constraint, although we avoid this terminology since it is suggestive of evolution, which we do not study.

(15) For example, the authors previously used the LOK model to show that thermal fluctuations alone can cause LER and LWR; cf. Patrone, P. N.; Gallatin, G. M., Macromolecules **2012**, *45*, 9507–9516. See also Bosse, A. W., Macromol. Theory Simul. **2010**, *19*, 399–406, and Bosse, A. W.; Lin, E. K.; Jones, R. L.; and Karim, A., Soft Matter **2009**, *5*, 4266-4271. For other works that discuss sources of fluctuations, see Semenov, A., N., Macromolecules **1994,** 27, 2732–2735; Stein, G. E.; Liddle, J. A.; Aquila, A. L.; Gullikson, E. M., Macromolecules **2010**, *43*, 433–441.

(16) From a modeling perspective, this distinction is important. The LOK model was originally intended to describe mean-field, or average properties of BCPs, as opposed to thermal fluctuations (although it has also been used for this purpose as well).[15] Here we describe the *average* behavior of a BCP thin film subject to boundary conditions with fluctuation.

(17) Cheng, J. Y. (moderator); Tong, W. M. (moderator) Panel Discussion on Challenges for Directed Self-Assembly. Presented at the SPIE Alternative Lithographic Technologies V Conference, San Jose, CA, 2013.

(18) Wang, Q.; Nath, S. K.; Graham, M. D.; Nealey, P. F.; de Pablo, J. J., J. Chem. Phys. **2000**, *112* 9996-10011.

(19) Liu, C.-C.; Ramírez-Hernández, A.; Han, E., Craig, G. S. W.; Tada, Y.; Yoshida, H.; Kang, H.; Ji, S.; Gopalan, P.; de Pablo, J. J.; and Nealey, P. F., Macromolecules **2013**, *46*, 1415–1424.

(20) Hur, S.-M.; Frischknecht, A. L.; Huberb, D. L.; Fredrickson, G. H., Soft Matter **2011**, *7*, 8776–8788.

(21) Stoykovich, M. P.; Daoulas, K. C.; M*ü*ller, M.; Kang, H.; de Pablo, J. J.; Nealey, P. F., Macromolecules **2010**, *43*, 2334–2342.

(22) Perera, G. M.; Wang, C.; Doxastakis, M.; Kline, R. J.; Wu, W.; Bosse, A. W.; Stein, G. E., Macro Lett. **2012**, *1*, 1244–1248.

(23) Wu, X.; Dzenis, Y. A., J. Chem. Phys. **2006**, *125*, 174707.

(24) Daoulas, K. C.; M*ü*ller, M.; Stoykovich, M. P.; Kang, H.; de Pablo, J. J.; Nealey, P. F., Langmuir **2008**, *24*, 1284–1295.

(25) Pereira, G. G.; Williams, D. R. M., Langmuir **1999**, *15*, 2125-2129; J. Chem. Phys. **1999**, *110*, 9223–9229.

(26) Matsen, M. W.; Schick, M., Phys. Rev. Lett. **1994**, *72*, 2660–2663.

(27) Finding an exact solution to the LOK model (not to mention more complex theories) is a task that evaded even the scientists that originally proposed it.

(28) Practically speaking, $|f| \ll \ell$ can be interpreted as $|f| \lesssim \ell/2$, provided the interface width $\xi \ll \ell$. This condition allows the solution $\hat{\phi}$ to reach its asymptotic values of ± 1 in the interior of any microdomain. If $|f| \gtrsim \ell/4$, the trial function given by Eq. (4) might not approximate the minimizer of the LOK functional.

(29) Mathematically, this is referred to as a "natural" boundary condition.

(30) Choksi, R.; Ren, X., J. Stat. Phys. **2003**, *113*, 151–176.

For Table of Contents Use Only

Response of Block-Copolymer Thin-Film Morphology to Line-Width Roughness on a Chemoepitaxial Template

Paul N. Patrone and Gregg Gallatin